

Add ^{10}Li luego de ^{10}Be

corrected 27/7/19

Chapter 6

Structure with transfer

Gregory write answer comments Ben

In what follows, we apply the formalism worked out in the previous chapters with the help of software developed to calculate absolute one- and two-particle transfer differential cross sections, to analyze reactions induced by both light and heavy ions (see App. 6.C COOPER, ONE). A number of examples are considered covering nuclei throughout the mass table. Namely, two-particle transfer ~~reactions~~ on ^{10}Be , as well as two-particle transfer on ^7Li , ^{11}Li , ^{48}Ca , and ^{206}Pb (systems around closed shells), and on open shell superfluid medium heavy nuclei (Sn-isotopes).

one particle transfer reactions on ^9Li and ^{10}Be , and

6.1 · The $^1\text{H}(^{11}\text{Li}, ^9\text{Li})^3\text{H}$ reaction: evidence for phonon mediated pairing

We start by discussing the analysis of the two-neutron pickup¹ reaction $^1\text{H}(^{11}\text{Li}, ^9\text{Li})^3\text{H}$. Particular attention is paid to the excitation of the $1/2^-$ first excited state of ^9Li lying at 2.69 MeV (see Figs. 1.9.4 and 6.1.1)². The results provide evidence for a new mechanism of pairing correlations in nuclei: pygmy resonance (low-energy $E1$ -strength) mediated pairing interaction³, which strongly renormalizes the bare, $NN \rightarrow ^1S_0$ interaction. This is but a particular embodiment of phonon mediated pairing interaction found throughout in nuclei⁴. The main difference between light halo exotic nuclei and medium heavy superfluid nuclei lying along the valley of stability is the role fluctuations play in dressing particles (quasiparticles) and in renormalizing their properties (mass, charge, etc.) and their interactions. In fact, in the case of e.g. Sn isotopes, mean field effects are dominant, while in the case of halo exotic nuclei renormalization effects can be as large as mean field ones. Concerning the pairing interaction, bare and induced contributions are about equal in the case of i.e. Sn-isotopes, while the second one is the overwhelming contri-

¹Tanihata, I. et al. (2008).

²To assess the direct character of the $1/2^-$ excitation process, the importance of inelastic and knockout (cf. Ch.4) channels were considered and found to be small (see App. 6.B).

³Barranco, F. et al. (2001); Potel et al. (2010).

⁴See e.g. Barranco et al. (1999); Gori et al. (2004) cf. also Brink, D. and Broglia (2005).

correct fig. see next page

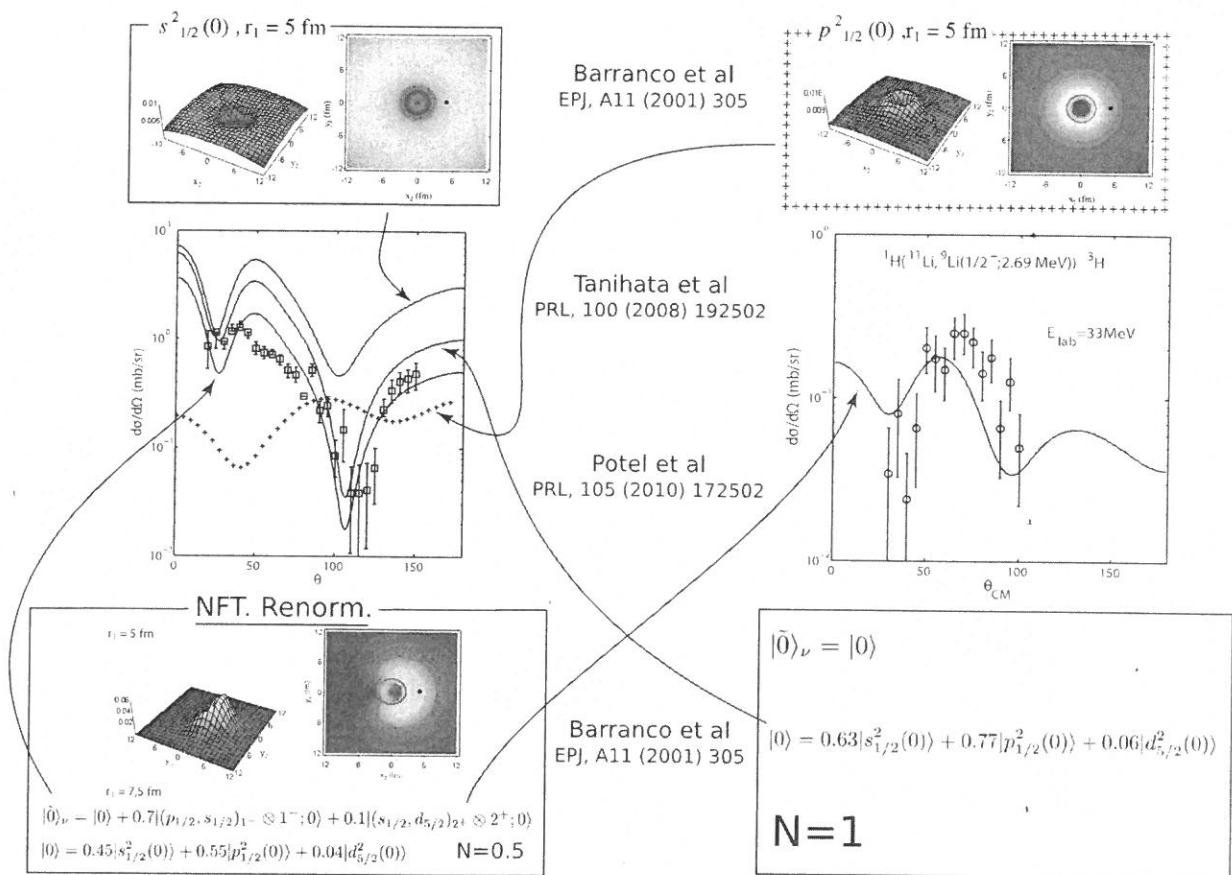


Figure 6.1.3: Absolute, two-nucleon transfer differential cross section associated with the ground state and the first excited state of ${}^9\text{Li}$, excited in the reaction ${}^1\text{H}({}^{11}\text{Li}, {}^9\text{Li}) {}^3\text{H}$ (Tanihata, I. et al., 2008) in comparison with the predicted differential cross sections (Potel et al., 2010) worked out making use of spectroscopic amplitudes and Cooper pair wavefunctions calculated with NFT, and of the optical potential collected in Table 6.1.1.

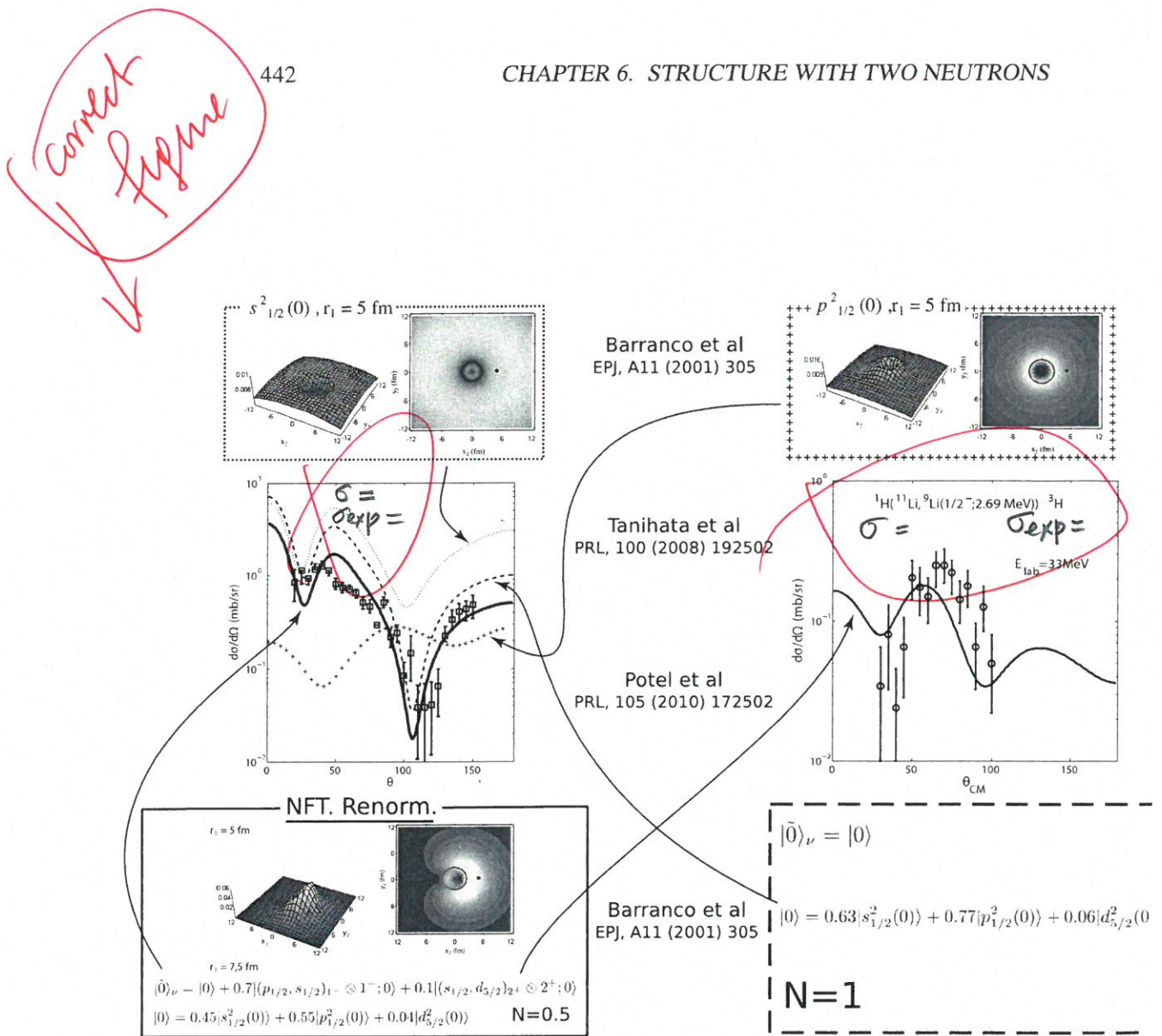


Figure 6.1.3: Absolute, two-nucleon transfer differential cross section associated with the ground state and the first excited state of ${}^9\text{Li}$, excited in the reaction ${}^1\text{H}({}^{11}\text{Li}, {}^9\text{Li}){}^3\text{H}$ (Tanahata, I. et al., 2008) in comparison with the predicted differential cross sections (Potel et al., 2010) worked out making use of spectroscopic amplitudes and Cooper pair wavefunctions calculated with NFT, and of the optical potential collected in Table 6.1.1.

bution in the case of ^{11}Li . The collective modes acting as glue of the Cooper pairs are mainly of quadrupole type in Sn and of dipole (pygmy resonance) type in the case of Li.

6.1.1 Structure

Within the scenario presented in Chapter 2 (Sect. 2.6) and Chapter 4 (Sect. 4.2.2) the wavefunction describing the structure of the halo neutrons in the ground state of ^{11}Li (the $p_{3/2}$ proton being assumed to act only as a spectator) can be written as

$$|0\rangle_v = |0\rangle + \alpha|(p_{1/2}, s_{1/2})_{1^-} \otimes 1^-; 0\rangle + \beta|(s_{1/2}, d_{5/2})_{2^+} \otimes 2^+; 0\rangle, \quad (6.1.1)$$

with

$$\alpha = 0.7, \quad \text{and} \quad \beta = 0.1, \quad (6.1.2)$$

and

$$|0\rangle = 0.45|s_{1/2}^2(0)\rangle + 0.55|p_{1/2}^2(0)\rangle + 0.04|d_{5/2}^2(0)\rangle, \quad (6.1.3)$$

$|1^-\rangle$ and $|2^+\rangle$ being the (RPA) states describing the dipole pygmy resonance of ^{11}Li and the quadrupole vibration of the core. The corresponding NFT diagrams are shown in diagrams (a), (d) and (e) of Fig. 1.9.4 (see also Fig. 2.6.3). The wavy curve represents both the quadrupole and dipole collective vibrational states being exchanged between the two halo neutrons, the horizontal dashed line the bare nuclear pairing interaction.

$^{11}\text{Li}(p, t)^9\text{Li}$												
	V	W	V_{so}	W_d	r_1	a_1	r_2	a_2	r_3	a_3	r_4	a_4
$p, {}^{11}\text{Li}^d$	63.62	0.33	5.69	8.9	1.12	0.68	1.12	0.52	0.89	0.59	1.31	0.52
$d, {}^{10}\text{Li}^b$	90.76	1.6	3.56	10.58	1.15	0.75	1.35	0.64	0.97	1.01	1.4	0.66
$t, {}^9\text{Li}^c$	152.47	12.59	1.9	12.08	1.04	0.72	1.23	0.72	0.53	0.24	1.03	0.83

Table 6.1.1: Optical potentials (cf. Tanihata, I. et al. (2008)) used in the calculation of the absolute differential cross sections displayed in Fig. 6.1.3 and Table 6.1.2.

$^{11}\text{Li}(p, t)^9\text{Li}$												
	V	W	V_{so}	W_d	r_1	a_1	r_2	a_2	r_3	a_3	r_4	a_4
$p, {}^{11}\text{Li}^d$	63.62	0.33	5.69	8.9	1.12	0.68	1.12	0.52	0.89	0.59	1.31	0.52
$d, {}^{10}\text{Li}^b$	90.76	1.6	3.56	10.58	1.15	0.75	1.35	0.64	0.97	1.01	1.4	0.66
$t, {}^9\text{Li}^c$	152.47	12.59	1.9	12.08	1.04	0.72	1.23	0.72	0.53	0.24	1.03	0.83

Table 6.1.2: Integrated two-neutron differential cross sections associated with the reaction ${}^1\text{H}({}^{11}\text{Li}, {}^9\text{Li}(i)){}^3\text{H}$ populating the ground state and the first excited state of ${}^9\text{Li}$ (Tanihata, I. et al. (2008), column labeled Experiment). The theoretical values are from Potel et al. (2010) (see also Potel, G. et al. (2013a)). See Figs. 6.1.3 and 6.B.2.

We are then in presence of a paradigmatic nuclear embodiment of Cooper's model which is at the basis of BCS theory: a single weakly bound neutron pair on top of the Fermi surface of the ${}^9\text{Li}$ core. But the analogy goes beyond these aspects, and covers also the very nature of the interaction acting between Cooper pair partners. Due to the the high polarizability of the system under study and of the small overlap of halo and core single particle wavefunctions, most of the Cooper pair correlation energy stems, according to NFT, from the exchange of collective vibrations, the role of the strongly screened bare interaction being, in this case, minor and (see Sect. 2.6). In other words, we are in the presence of a new realization of the Cooper model in which a totally novel Bardeen-Pines-Fröhlich-like phonon induced interaction is generated by a self induced collective vibration of the nuclear medium.

$({}^9\text{Li}) \quad i.e \quad |1/2^-, 2.69\text{ MeV}({}^9\text{Li})\rangle$

In connection with (6.1.1), it is revealing that the two states populated in the inverse kinematics, two-neutron pick up reaction ${}^1\text{H}({}^{11}\text{Li}, {}^9\text{Li}){}^3\text{H}$ are⁵, the $|3/2^-\text{gs}({}^9\text{Li})\rangle$ and the first excited $|1/2^-, 2.69\text{MeV}\rangle$ level of ${}^9\text{Li}$ (see Figs. 1.9.4 (f) and 6.1.1 and - 6.1.3).

~~6.1.2~~ The associated absolute differential cross sections calculated making use of the spectroscopic amplitudes displayed in (6.1.1)–(6.1.3) and the optical potentials displayed in ... provide a quantitative account of the experimental data within the NFT scenario, the $|0\rangle$ and the $|(\ell_{1/2}, d_{5/2})_{2+} \otimes 2^+; 0\rangle$ component of the Cooper pair wavefunction⁶ respectively. The outcome of acting with the two-particle transfer field on the $|(\ell_{1/2}, s_{1/2})_{1-} \otimes 1^-; 0\rangle$ component is expected to lead to non-collective particle-hole-like excitation, unlikely to carry enhanced cross sections. On the other hand, this component plays, through normalization, a central role in the value of the absolute cross section of the populated states. In particular, concerning the ground state (Fig. 6.1.3)

Table 6.1.1,

(Fig. 6.1.3) 6.1.2 Reaction

Because second order calculations of inelastic, break up and final state interaction channels, which in principle can provide alternative routes for the population of the first excited state of ${}^9\text{Li}$ (see Fig. 6.B.1 and Table 6.B.1) to the direct one predicted by the wavefunction (6.1.1) (β component), lead to absolute cross sections which are smaller by few orders of magnitude than that shown in Fig. 6.1.3, one can posit that quadrupole core polarization effects in $|\text{gs}({}^{11}\text{Li})\rangle$ is essential to account for the observation of the $|1/2^-, 2.69\text{ MeV}\rangle$ state, thus providing evidence for phonon mediated pairing in nuclei.

The reason why in the case of ${}^{11}\text{Li}$ evidence for phonon mediated pairing is, arguably, inescapable, is connected with the fact that reaching the limits of stability associated with drip line nuclei, the system also reaches to situations in which medium polarization effects become overwhelming. In fact, one is, in such cases confronted with elementary modes of nuclear excitation in which dynamic fluctuation effects are as important as static, mean field effects. Within this context we

⁵Tanikata, I. et al. (2008).

⁶Fig. 6.1.2, see also Figs 4.2.5 and ??, see also Figs. 6.1.3 and 2.6.3.

refer to parity inversion (see Figs. 2.6.3 and 6.2.1). Nuclear field theory allows one to sum to infinite order little convergent processes⁷ and is thus specially suited to study halo systems⁸. From these studies it emerges a possible new elementary mode of excitation, namely pair addition halo vibration, of which $|\text{gs}({}^{11}\text{Li})\rangle$ state is a concrete embodiment. It is associated with a novel mechanism for stabilizing Cooper pairs, which arises from a (dynamical) breakup of gauge invariance (see App. 6.A). Their most distinctive feature, namely that of carrying on top of it a (dipole) pygmy resonance at a relative excitation energy of about 1 MeV, a necessary although not sufficient condition for this new mode to exist, can be instrumental for its characterization. While neutron pair addition mode is in the case of ${}^9\text{Li}$ the ground state, in other nuclei it may be an excited state which could be observed in a combined $L = 0$, and $L = 1$, two-particle transfer reaction to excited states, or in terms of $E1$ decay of the soft mode (pygmy resonance) built on top of it. Within this context, it is an open question whether one could expect to find a realization of such a halo pair addition mode in, for example, the first excited 0^+ state of ${}^{12}\text{Be}$ (see Fig. 6.1.4).

Single-particle $s_{1/2}$ and $p_{1/2}$ states at threshold in neutron drip-line nuclei have been found to lead, within the framework of a bare, short range, pairing interaction scheme to halo anti-pairing effects⁹. The fact that the two-neutron separation energy of the halo neutrons (halo Cooper pair) of ${}^{11}\text{Li(gs)}$ is $\approx 400\text{keV}$, testifies to the fact that the anti-halo pairing effect is, in this case, overwhelmed by (dynamical) medium polarization effects.

Within this context it is of notice that, again, the interweaving of the different elementary modes of nuclear excitation, pairing and dipole pygmy resonances in the present case, condition reaction studies, let alone the possibility to study (pygmy) giant resonances built on excited states, and to provide a novel test of the Brink-Axel hypothesis which is at the basis of the statistical description of photon decay from hot (compound) nuclei¹⁰.

Before concluding this section we provide in Fig. 6.1.5 examples of pairing vibrational states around ${}^9\text{Li}$, ${}^{10}\text{Be}$, ${}^{48}_{20}\text{Ca}_{28}$ and ${}^{208}_{82}\text{Pb}_{126}$, $N = 6$, $N = 28$ and $N = 126$ neutron closed shell systems. The fact that among the (p, t) and (t, p) absolute differential cross sections one also finds the ${}^{208}\text{Pb}({}^{16}\text{O}, {}^{18}\text{O}){}^{206}\text{Pb(gs)}$ absolute differential cross section is in keeping with the fact that the formalism to treat both light and heavy ions two-nucleon transfer reactions and their connection is well known¹¹ and rather homogeneous¹². Thus, it has been implemented in the software COOPER as a standard option (cf. App. 6.C). As observed, theory provides

⁷Bortignon, P. F. et al. (1978).

⁸Barranco, F. et al. (2001) and Gori et al. (2004).

⁹Bennaceur, K. et al. (2000), cf. also Hamamoto and Mottelson (2003). Hamamoto, I. and Mottelson (2004).

¹⁰cf. Axel (1962), Brink (1955 (unpublished); cf. also Bortignon, P. F. et al. (1998), Bertsch, G. F. and Broglia (1986) and references therein.

¹¹Broglia and Winther (2004), Bayman and Chen (1982) and Thompson (1988) and references therein.

¹²Poté, G. et al. (2013b).

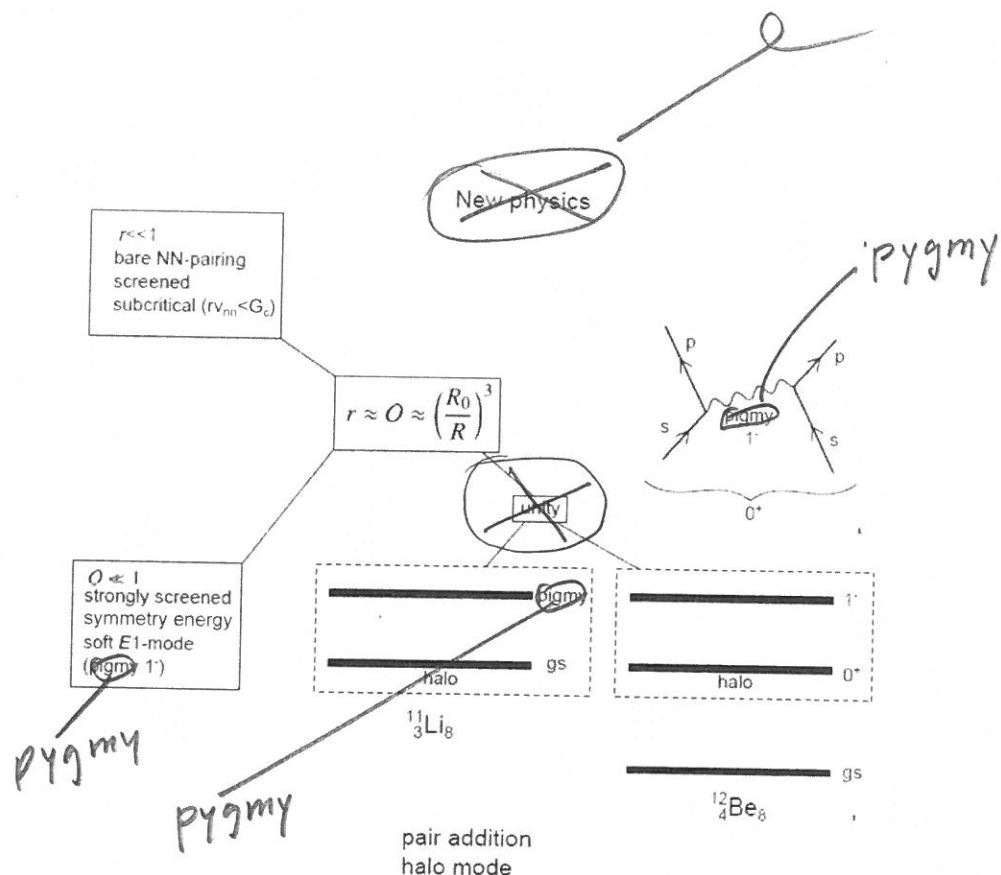


Figure 6.1.4: Schematic representation of a possible realization of halo pair addition mode in terms of the first excited 0^+ state (2.24 MeV) of ^{12}Be (for details see Sect. 2.6).

In Table 6.4.1 we collect the two-nucleon spectroscopic amplitudes associated with the reactions $^{A+2}\text{Sn}(p,t)^A\text{Sn}$, for A in the interval 112–126. Making use of these results and of global optical parameters (see Table 6.4.2), the absolute differential cross section $^{A+2}\text{Sn}(p,t)^A\text{Sn}(\text{gs})$ were calculated. They are shown in Fig. 6.4.1 in comparison with the data.

	^{112}Sn	^{114}Sn	^{116}Sn	^{118}Sn	^{120}Sn	^{122}Sn	^{124}Sn
$1d_{5/2}$	0.664	0.594	0.393	0.471	0.439	0.394	0.352
$0g_{7/2}$	0.958	0.852	0.542	0.255	0.591	0.504	0.439
$2s_{1/2}$	0.446	0.477	0.442	0.487	0.451	0.413	0.364
$1d_{3/2}$	0.542	0.590	0.695	0.706	0.696	0.651	0.582
$0h_{11/2}$	0.686	0.720	1.062	0.969	1.095	1.175	1.222

Table 6.4.1: Two-nucleon transfer spectroscopic amplitudes $\langle BCS(A)|P_\nu|BCS(A+2) \rangle = \sqrt{(2j_\nu + 1)/2} U_\nu(A)V_\nu(A+2)$, associated with the reactions connecting the ground states (members of a pairing rotational band) of two superfluid Sn-nuclei $^{A+2}\text{Sn}(p,t)^A\text{Sn}(\text{gs})$ (Potel, G. et al. (2013a,b)).

	$^A\text{Sn}(p,t)^{A-2}\text{Sn}$											
	V	W	V_{so}	W_d	r_1	a_1	r_2	a_2	r_3	a_3	r_4	a_4
$p, {}^A\text{Sn}^a)$	50	5	3	6	1.35	0.65	1.2	0.5	1.25	0.7	1.3	0.6
$d, {}^{A-1}\text{Sn}^b)$	78.53	12	3.62	10.5	1.1	0.6	1.3	0.5	0.97	0.9	1.3	0.61
$t, {}^{A-2}\text{Sn}^a)$	176	20	8	8	1.14	0.6	1.3	0.5	1.1	0.8	1.3	0.6

Table 6.4.2: Optical potentials (see caption Fig. 6.4.1) used in the calculations of the absolute differential cross sections displayed in Fig. 6.4.1.

this figure.

6.4.1 Structure-reaction: stability of the order parameter α_0

As discussed before, the order parameter associated with distortion in gauge space can be written as

$$\alpha'_0 = \sum_{j_a} \sqrt{\frac{2j_a + 1}{2}} B(j_a^2(0), N \rightarrow N + 2), \quad (6.4.1)$$

where

$$B(j_a^2(0), N \rightarrow N + 2) = \sqrt{\frac{2j_a + 1}{2}} U'_{j_a}(N) V'_{j_a}(N + 2) \quad (6.4.2)$$

is the two-nucleon spectroscopic amplitude associated with the ($j^2(0)$) pair transfer between members of a pairing rotational band. Thus

$$\alpha'_0 \approx \sum_{j_a} \frac{2j_a + 1}{2} U'_{j_a} V'_{j_a} = e^{-2i\phi} \sum_{j_a} \frac{2j_a + 1}{2} U_{j_a} V_{j_a} = e^{-2i\phi} \alpha_0, \quad (6.4.3)$$

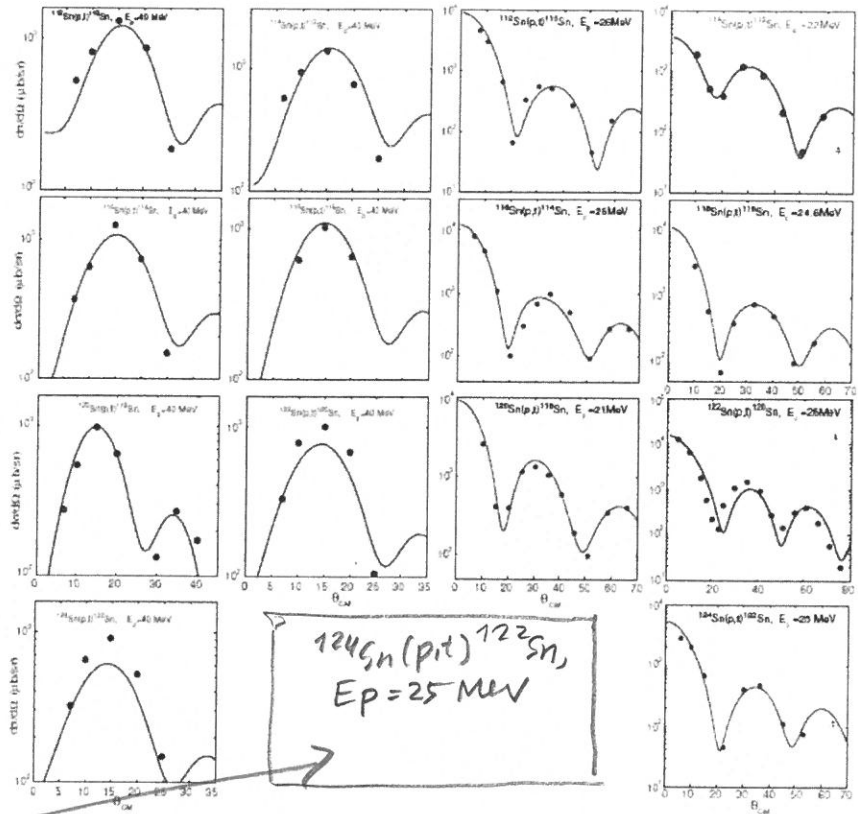
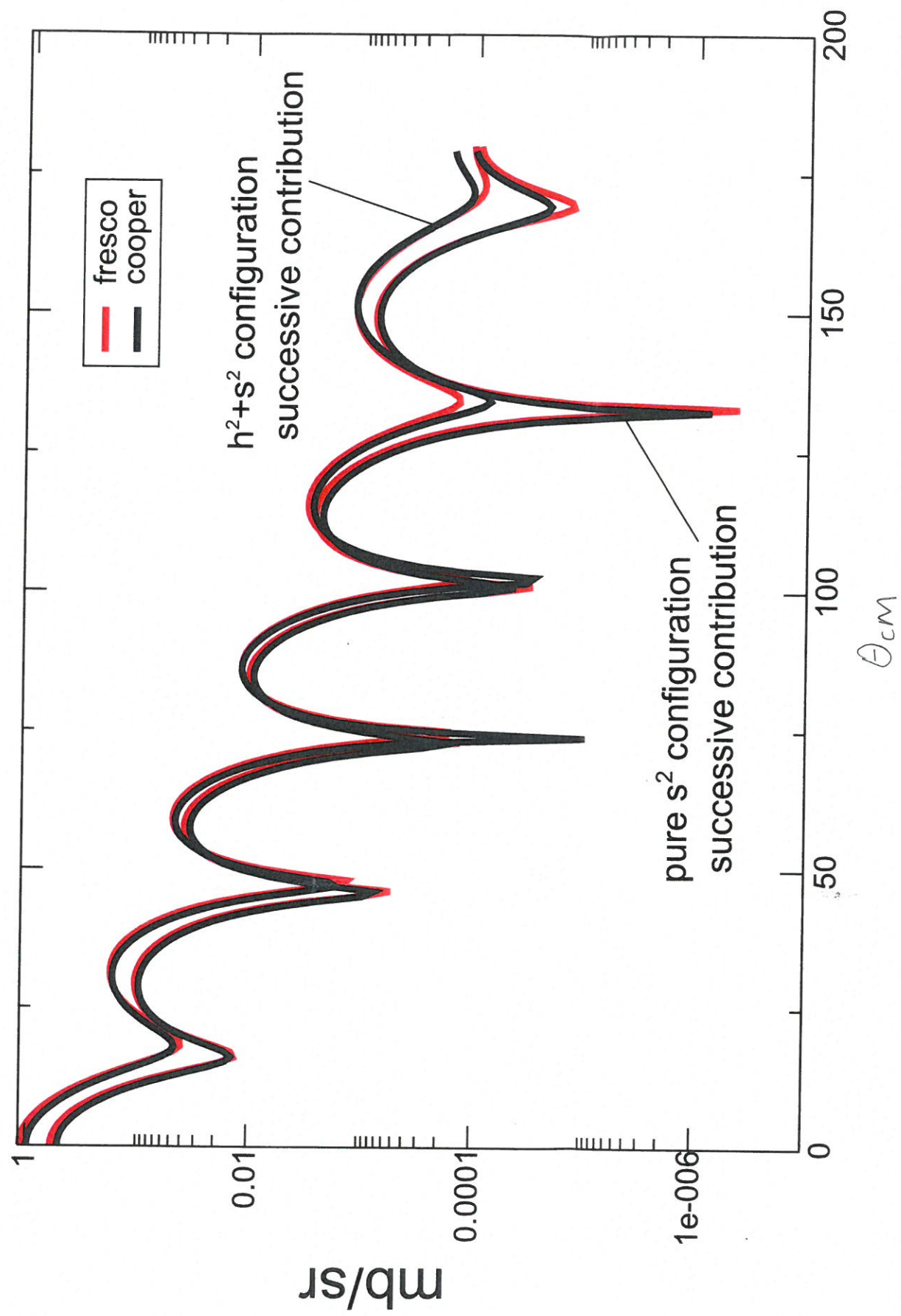


Figure 6.4.1: Predicted (continuous curve, Potel, G. et al. (2013a,b)) absolute differential $^{A+2}\text{Sn}(p,t)^A\text{Sn(gs)}$ cross sections for bombarding energies $E_p=40$ MeV (in the two left columns) and $21 \text{ MeV} \leq E_p \leq 26 \text{ MeV}$ (in the two right columns) in comparison with the experimental data (solid dots, Bassani et al. (1965), Guazzoni, P. et al. (1999), Guazzoni, P. et al. (2004), Guazzoni, P. et al. (2006), Guazzoni, P. et al. (2008), Guazzoni, P. et al. (2011), Guazzoni, P. et al. (2012)).

See next page

In the center of the lowest row, ~~is displayed in the angular interval~~ ^{displayed in the angular interval} $0^\circ \leq \theta \leq 200^\circ$ ~~comparison between the absolute differential cross section (successive transfers) associated with the process~~ $^{124}\text{Sn}(p,t) ^{122}\text{Sn}(f)$ ~~in comparison with the software COOPER and FRESCO (Thompson (1))~~ $(f = h_{1/2}^2(0), s_{1/2}^2(0))$ calculated with both the results worked out are displayed.

$^{124}\text{Sn}(p,t)^{122}\text{Sn}$, $E_p = 25 \text{ MeV}$



(see also Fig. 6.6.1)

As shown in Fig. 6.6.2, the reaction $^{11}\text{Be}(p, d)^{10}\text{Be}(2^+)$ provides another embodiment of such processes. In fact, this reaction gives information concerning the most important process clothing of the $1/2^+$ parity inverted ground state of $^{11}_4\text{Be}_7$ through the coupling to the low-lying quadrupole vibration of the core $^{10}_4\text{Be}_6$ (see I (a)). A schematic representation of the pickup of the neutron moving around a $N = 6$ closed shell and populating the low-lying quadrupole vibrational state of this core, in coincidence with the corresponding γ -decay is shown in I(b). More detailed structure and reaction NFT diagrams, are shown in I(d) and I(e), (the jagged line represents a graphic mnemonic of the recoil effect), together with a cartoon representation in (f). The predicted (continuous curve) and experimental (solid dots) absolute differential cross sections are displayed in I(c). In I(a)-(e), protons and neutrons are labeled π and ν respectively, while d stands for deuteron. Particle detectors are drawn as hatched rectangles while γ -detectors are represented by a crossed rectangle. Curved arrows indicate motion in the continuum (reaction). Normal arrowed lines, motion inside target or projectile (structure).

At the basis of the spontaneous γ -decay displayed in I(b) and I(e) we find the processes shown in II. The solid dot represents the interaction of nucleons in general and of protons in particular with nuclear vibrations, while a normal vertex represents the interaction of photons and protons. The variety of diagrams shown have general validity. Nonetheless it was assumed that one is dealing with the low-lying correlated particle-hole quadrupole vibration ($L = 2$) of $^{10}_4\text{Be}_6$ lying at 3.368 MeV and displaying a $B(E2; 0^+ \rightarrow 2^+) = 0.0052 e^2 b^2$ ($\beta_2 \approx 0.9$). In II(a) and (b), the zero point fluctuations of the nuclear ground state associated with nuclear vibrations, and with the electromagnetic field are shown, while in II (c) Pauli principle correction to the simultaneous presence of the above two ZPF processes are displayed. As shown in (d), intervening the virtual excitation of the nuclear vibrations with an external (inelastic) field (cross followed by a dashed line), the virtual process (c) becomes real, the γ -ray eventually bringing this information to the detector. Diagrams II (e) and (f) show the time ordering of the above process and describe the RPA contributions, through backwardsgoing and forwardsgoing amplitudes, of the spontaneous γ -decay of the quadrupole vibration of ^{10}Be .

The above example, aside from shedding light on retardation mechanisms in clothing processes, implies that particle-vibration coupled intermediate states have to be real concerning both energy and amplitude, as well as radial shape²⁴. Thus $(\text{NFT})_{\text{ren}}$ is not a calculation ansatz but a quantal requirement. From here the reason to draw with bold face lines and curves belonging to intermediate states.

6.5.2 On-shell energy

It was stated that intermediate states are built out, aside from their energy, of a fully dressed, renormalized physically observable elementary modes of excitation. Concerning the eventual value of the on-shell-energy, it will naturally depend on

empirical input. Thus, empirical renormalization.

²⁴See e.g. Barranco et al. (2017).

overall centroid of the valence orbitals as well as the density of levels associated with the two potentials. Within this context it is of notice that the Lamb (-like) shift taking place between the $s_{1/2}$ and $p_{1/2}$ valence levels of ^{11}Be has a value of approximately 10% ($(\Delta\epsilon_{1/2^+,1/2^-})_{\text{bare}} - (\Delta\epsilon_{1/2^+,1/2^-})_{\text{ren}} \approx 3.11 + 0.32\text{MeV}$) of that of the Fermi energy ($\approx 36\text{ MeV}$). This result can be compared with the ratio of the hydrogen $^2S_{1/2} - ^2P_{1/2}$ Lamb shift ($1058\text{ MHz} \approx 4.3 \times 10^{-9}\text{ eV}$) and the Rydberg constant ($R_H = 13.6\text{ eV}$), i.e. $\approx 10^{-10}$, a result which underscores the strong coupled situation one is confronted with in trying to describe the structure of light halo exotic nuclei (Fig. 6.2.1).

6.6.1 One-particle transfer and optical potential

The fact that in spite of this non-perturbative situation, $(\text{NFT})_{\text{ren}}(\mathbf{r}+\mathbf{s})$ can provide an overall account of an essentially complete set of experimental data which characterizes ^{11}Be , within a 10% error, testifies to the power and flexibility Feynman version of Q.E.D. has. It can be used as paradigm to construct a field theory for both structure and reactions of a strongly interacting finite many-body system like the atomic nucleus. As already mentioned, examples of $(\text{NFT})_{\text{ren}}(\mathbf{r}+\mathbf{s})$ diagrams, aside from that discussed in detail in connection with Fig. 6.6.2, are displayed in Figs. 1.9.3 and 1.9.2. The first describes the process $^1\text{H}(^{11}\text{Li}, ^9\text{Li})^3\text{H}$ providing a quantitative account of the data and first evidence of phonon induced pairing in nuclei. The second shows in (a), one of the most important channels contributing to the optical potential needed to describe the elastic scattering process $^1\text{H}(^{11}\text{Li}, ^{11}\text{Li})^1\text{H}$.

~~Processes taking place between $t_1 - t_7$ are described below. First, the halo pair addition mode $|0_v^+\rangle$ decays at time t_1 into a pure two-particle configuration. Its binding to the ^9Li core is related to parity inversion where the $s_{1/2}$ continuum orbital is lowered to threshold through cloaking with mainly quadrupole vibrational modes and the $p_{1/2}$ bound state suffers a strong repulsion into a resonant state by Pauli principle with particles participating in the quadrupole mode. The resulting dressed two-neutron states get bound mainly through the exchange of the 1^- giant dipole pygmy resonance (GDPR), represented for simplicity, as a correlated particle hole excitation (wavy line labeled 1^-). The bare pairing interaction (horizontal dotted line acting at t_7) contributing subcritically to the binding process. At time t_8 , one of the neutrons of the halo Cooper pair is transferred, with the emission of a recoil mode, to the incoming proton projectile through the proton-neutron interaction v_{np} (prior representation), leading to a deuteron. This neutron is, at time t_9 transferred back (to virtual ^{10}Li) through v_{np} acting a second time (post representation), with the simultaneous absorption of the recoil mode. Eventually, at time t_{10} the two neutrons merge, through the particle-pair vibrational coupling, into the halo pair addition mode $|0_v\rangle$. These processes lead to polarization contributions to the $^9\text{Li} + p$ elastic scattering optical potential.~~

The calculation of the optical potential constitutes a major challenge lying ahead.

	V_0 (MeV)	V_l (MeV)	R_0 (fm)	a (fm)
Standard ^{a)}	-50	17	2.7 ^{c)}	0.65
bare ^{b)}	-68.9	14.47	2.15 ^{d)}	0.77

(Bohr and Mottelson (1969))

Table 6.6.1: Parametrization of the standard and of the bare mean field potential associated with ^{11}Be (Barranco et al. (2017)). Changes of the order of 20-30% are observed. Within this context, in the case of Q.E.D. $\delta m_e/m_e = 0.1$.

^{a)} $m^* = m$

^{b)} $m^*(r=0) = 0.7m$, $m^*(r=\infty) = 10/11m$

^{c)} $R_0 = r_0 A^{1/3}$, $r_0 = 1.2 \text{ fm}$

^{d)} $r_0 \approx 1.03 \text{ fm}$

tual excitation of the nuclear vibrations (graph (c)) with an external (inelastic) field (cross followed by a dashed line), in coincidence with the γ -decay (γ -detector, crossed box), the virtual process (c) becomes real. (e), (f) Time ordering of the above process correspond to the RPA contributions through backwardsgoing and forwardsgoing amplitudes and subsequent γ -decay.

move to
p. 469

(a)

6.6.3 The structure of “observable” Cooper pairs

In his Waynflete lectures on Cause and Chance, Max Born³¹, to whom we owe the statistical interpretation of quantum mechanics³², states “... quantum mechanics does not describe an objective state in an independent external world, but the aspect of this world gained by considering it from a certain subjective standpoint, or with certain experimental means and arrangements”. It is within this context that we tried in previous sections to get insight concerning the structure of nuclear Cooper pairs. Specifically, in terms of two-nucleon transfer reactions. Being even more *subjective* (concrete), we were interested in shedding light on the structure of one of the 5-6 Cooper pairs participating in the condensate (intrinsic state in gauge space) of the Sn-isotopes (ground state rotational band³³) through pair transfer processes. That is $A+2\text{Sn}(p,t)^A\text{Sn}(\text{gs})$ processes in general, and $^{120}\text{Sn}(p,t)^{118}\text{Sn}$ in particular. From a strict observational perspective, concerning Cooper pairs, one can only refer to the information two-nucleon transfer absolute differential cross sections carry on these entities. On the other hand, leaving the discussion regarding the microscopic calculation of the optical potential, the carriers mediating information between structure and differential cross sections, e.g. between target and outgoing particle in a standard laboratory setup, are the distorted waves. These functions can be studied independently of the transfer processes under consideration, in elastic

³¹Born (1948).

³²Born (1964); Pais (1986).

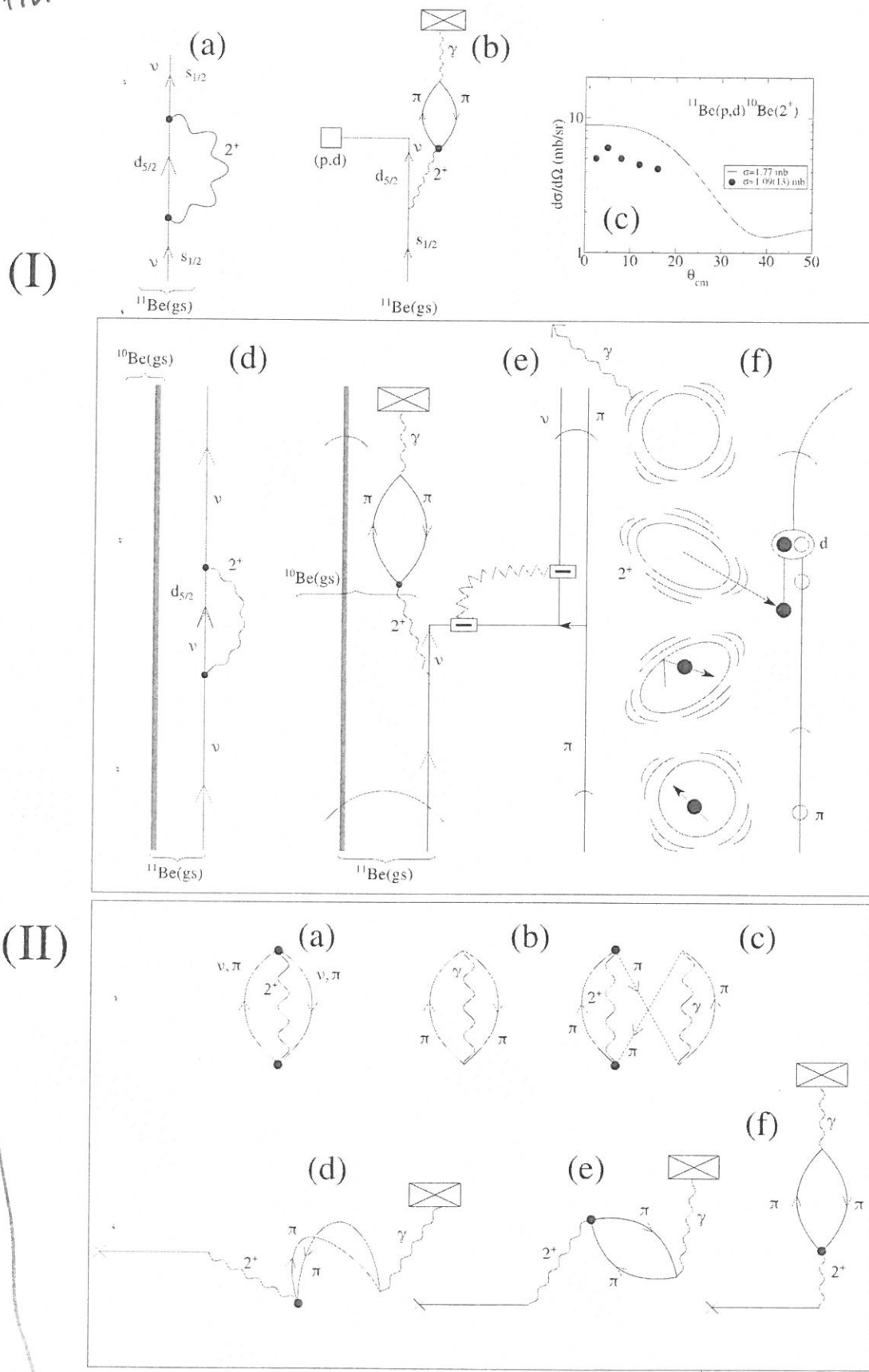
³³Potel, G. et al. (2013b); Potel et al. (2017)

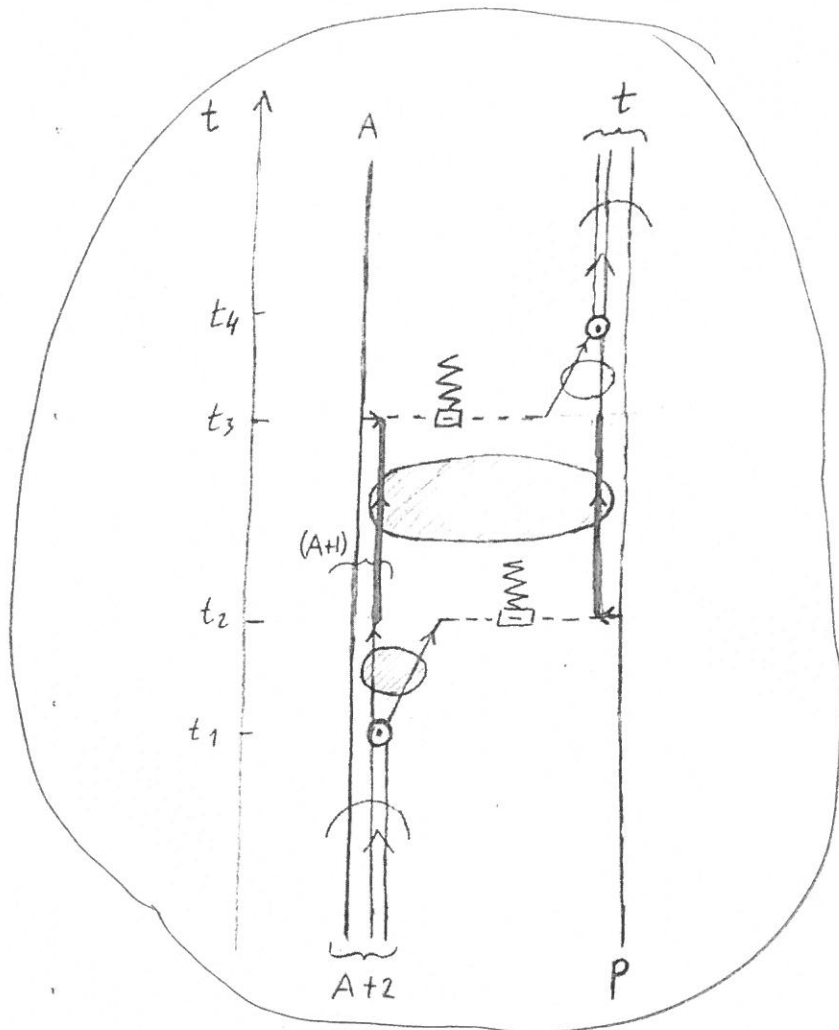
a virtual process, namely the self-energy contribution of the renormalization of the $5/2^-$ ground state of ^{11}Be through the coupling to the low-lying collective quadrupole vibration of the ^{10}Be become real through the action of a one-particle pickup external field.

6.6. PERTURBATION AND BEYOND

475

caption





reemplazar
Figura 8
EPJA Hawking
Corregida
ver p(477)
a

next
page

Figure 6.6.3: Diagram describing structure and reaction aspects of the main process through which a Cooper pair (di-neutron) tunnels from target to projectile in the reaction $(A + 2) + p \rightarrow A + t$. In order that the two-step process $(A + 2) + p \rightarrow (A + 1) + d \rightarrow A + t$ takes place, target and projectile have to be in contact at least in the time interval running between t_2 and t_3 . During this time, the two systems create, with local regions of ever so low nucleonic presence, a common density over which the non-local pairing field can be established, and the Cooper pair can be correlated. Even with regions in which the pairing interaction may be zero. Small ellipses (with linear dimensions of the order of the nuclear radius R_0) indicate situations in which the two neutron correlation is distorted by the external mean field of a single of the systems involved of the reaction, i.e. $A + 2$ in the entrance channel, t in the exit one (see e.g. Fig. 2.6.3). The large ellipse (with linear dimensions of the order of the correlation length ξ) indicate the region in which the two partners of the Cooper pair correlate over distances of the order of the correlation length ξ . It is this information that the outgoing particle of a Cooper pair transfer process brings to the detector. In other words, this is the observable Cooper pair in terms of its specific probe, and the reason why the neutrons are described, in the interval $\Delta t = t_3 - t_1$, in terms of bold face arrowed lines.

Let us now discuss the correlation between particles and holes (ph) associated with the two quasiparticle (pp, ph, hh) states 2_1^+ and 1^- , and at the basis of the phenomena of core polarization responsible for the dressing of particles (self energy) and the renormalization of the ph and (pp, hh) interactions (vertex and pairing renormalization).

As seen from figs. 7(middle part) and (lower part), the (ph) become closer together when correlated by the quadrupole and the dipole residual interaction, respectively. Emitted and reabsorbed by the same nucleons (fig. 3 insets (A) and (B), fig. 5(I)(a), (d), fig. 6(a)) they give rise to the quasiparticle degrees of freedom carrying effective masses (energies) and spectroscopic amplitudes (single-particle content), as experimentally observed (see e.g. [45, 46] and references therein). Exchanged between nucleons (fig. 6(b)) they renormalise the bare nucleon-nucleon interaction, in particular the 1S_0 pairing interaction (see e.g. [28, 29] and references therein), effects which can be treated in nuclear field theory also to infinite order of perturbation if needed, in particular in the case of superfluid nuclei, but also of halo nuclei like ^{11}Li . Ground state correlations of ph collective modes and associated renormalization effects provide non negligible contributions to the binding energies (see figs. 5(II)(a)–(c), table 1 and e.g. [40] and references therein). They are also essential in reproducing the experimental value of the electromagnetic transition probabilities. In fact, dressing the collective vibrations, e.g. the collective quadrupole mode of ^{120}Sn , leads to conspicuous increase in the $B(E2)$ value, associated with the decay into the ground state [69], in overall agreement with the experimental findings.

Clearly, this can hardly be connected with whether particles and holes are close in space, as the wavelength of γ -rays of 1–2 MeV are orders of magnitude larger than nuclear dimensions. In fact, it is related to the fact that the components of the wavefunctions of collective states are phase-correlated, as is the case in pp correlated states (pairing vibrations like $|^{11}\text{Li}(\text{gs})\rangle$) and associated two-particle, mainly successive, transfer.

A summary of correlation and entanglement simultaneously operative at the level of structure and reaction discussed above, is shown in fig. 8, for the case of the process $A+2X + p \rightarrow A X(J^\pi; E_x) + t$ (e.g. $^{11}\text{Li} + p \rightarrow ^9\text{Li}(1/2^-; 2.69 \text{ MeV}) + t$). The small (grey) ellipses focus on the particle-particle (neutron-neutron) correlations. That is, a structure property which is calculated for the systems $(A+2)$ and t ($\equiv ^3\text{H}$) in isolation. The corresponding wavefunctions describe the effect of both (pp)-correlation (weak), as well as that of the single-particle field (strong). The large ellipse focus on the (pp) entanglement opera-

¹¹⁶Sn + ⁶⁰Ni at energies far below the Coulomb barrier are equal within experimental errors, from the (smallest) safe distance of closest approach $d \approx 12 \text{ fm}$ to a value $d \approx 13.2 \text{ fm}$ consistent with the Cooper pair correlation length in ^{116}Sn ($\xi = \frac{\hbar v_F}{\pi \Delta} \approx 12.3 \text{ fm}$, $\Delta \approx 1.4 \text{ MeV}$, $v_F/c = 0.27$). The main proviso being related with the fact that the reported are values referred to inclusive reaction cross sections ($E_x \lesssim 2 \text{ MeV}$; in the case of pair transfer σ (exc. states) $\lesssim 24\%$ of the total cross section).

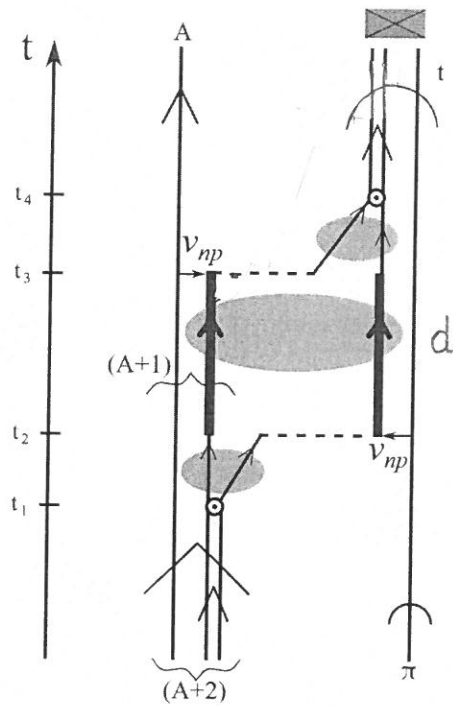


Fig. 8. General nuclear field theory diagram describing structure and reaction aspects of the main process through which a Cooper pair (di-neutron) tunnels from target to projectile in the reaction $(A+2) + p \rightarrow A + t$. In order that the two-step process $(A+2) + p \rightarrow (A+1) + d \rightarrow A + t$ takes place under the influence of the proton-neutron interaction v_{np} , target and projectile have to be in contact at least in the time interval running between t_2 and t_3 . During this time, the two systems create, with local regions of ever so low nucleonic presence, a common density over which the non-local pairing field can be established, and the Cooper pair can be correlated. Even with regions in which the pairing interaction may be zero. Small grey ellipses (with linear dimensions of the order of the nuclear radius R_0) indicate situations in which the two neutron correlation is distorted by the mean field of a single of the systems involved of the reaction, i.e. $A+2$ in the entrance channel, t in the exit one. This mean field can be viewed as acting as an external field. The large grey ellipse (with linear dimensions of the order of ξ) indicates the region in which the two partners of the Cooper pair correlate over distances of the order of the correlation length. It is this information that the outgoing particle of a Cooper pair transfer process brings to the detector. In other words, this is the closest to what can be defined as the observable Cooper pair in terms of its specific probe, i.e. two-nucleon transfer process, and the reason why the neutrons are described, in the interval $\Delta t = t_3 - t_1$, in terms of bold face arrowed lines. In the present case the diagram is tailored to describe the process shown schematically in fig. 6(c), i.e. $^{11}\text{Li}(p, t)^9\text{Li}(1/2^-)$. Namely a situation in which the irreversible event associated with the tunneling of the second fermion takes place before the collective vibration is either reabsorbed by it, or is exchanged with the first neutron, forcing the collective mode to become on-shell and, after coupling to the electromagnetic field, escape the reaction area, entangled (large light blue ellipse) with the two fermions (neutrons) which have fallen into the no-return field of the triton (see fig. 1(I)(b)).

6.B.1 (e) as well as Eqs. (6.1.1)–(6.1.3). In fact, and as shown in Figs. 6.B.2 and 6.B.3, the contributions of break up processes and inelastic (Figs. 6.B.1(f),(g) and (h) respectively) to the population of the $1/2^-$ (2.69 MeV) first excited state of ^9Li are negligible as compared with the process depicted in Fig. 6.B.1(e). In the case of the breakup channel (Figs. 6.B.1(f) and 6.B.1(g)) this is a consequence of the low bombarding energy of the ^{11}Li beam (inverse kinematics), combined with the small overlap between continuum (resonant) neutron $p_{1/2}$ wavefunctions and bound state wavefunctions. In the case of the inelastic process (Fig. 6.B.1(h)), it is again a consequence of the relative low bombarding energy. In fact, the adiabaticity parameters ξ_C, ξ_N ⁵¹ associated with Coulomb excitation and inelastic excitation in the $t+^9\text{Li}$ channel are larger than 1, implying an adiabatic cutoff. In other words, the quadrupole mode is essentially only polarized during the reaction but not excited. The situation is quite different in the case of the intervening of the virtual processes displayed in Fig. 6.B.1 (b) and (c) leading to the population of the $1/2^-$ state displayed in Fig. 6.B.1 (e). Being those off-the-energy shell processes, energy is not conserved, and adiabaticity gets profoundly modified.

Appendix 6.C Software

In this Appendix we provide a brief description of the numerical methods implemented in the code written to evaluate the differential cross sections. The two-nucleon transfer differential cross section is given by Eq. (5.1.4), so the principal task consist in calculating the transfer amplitudes $T^{(1)}(\theta)$, $T_{succ}^{(2)}(\theta)$ and $T_{NO}^{(2)}(\theta)$ described in Eqs. 5.1.5a–5.1.5c, by numerically evaluating the corresponding integrals. The dimensionality of the integrals can be reduced by expanding in partial waves (eigenfunctions of the angular momentum operator) the distorted waves and wavefunctions present in the corresponding integrands. The resulting expressions are Eqs. (5.2.36) and (5.2.37) for $T^{(1)}(\theta)$, Eqs. (5.2.128), (5.2.129) and (5.2.130) for $T_{succ}^{(2)}(\theta)$, and Eqs. (5.2.154), (5.2.155) and (5.2.156) for $T_{NO}^{(2)}(\theta)$. The integrals are computed numerically with the method of Gaussian quadratures.

The one-dimensional (radial) functions appearing in the integrands are defined in a spatial grid up to a given maximum radius r_{max} . The bound state wavefunctions are obtained by numerical integration of the radial Schrödinger equation for a Woods–Saxon potential with a spin-orbit term. The parameters defining the shape of the potential are given as an input, while the depth is adjusted to reproduce the binding energy of the state under consideration. The resulting potential corresponding to the final (initial) nucleon bound state stands also for the interaction potential featured in the integrand in the prior (post) representation. The distorted waves are obtained by integrating the radial Schrödinger equation with positive energy from $r = 0$ to r_{max} , and matching the solution with the corresponding Coulomb wave function at a given $r = r_{match}$, big enough to lie outside of the range of the nuclear interaction. The Woods–Saxon optical potentials used to obtain the distorted

⁵¹See eqs. (IV.12) and (IV.14) of ref. Broglia and Winther (2004).

← Gregory answer also
 B. Bayman
 comments
 and
 questions

for the denominator of Eq. (6.D.2). From the above results the correlation function between particle 1 and 2 is

$$\text{Corr} = \frac{2C}{\hbar\omega} \langle x_1 x_2 \rangle = 2\Re(\lambda^* \mu) = \begin{cases} 1 & (\lambda = +\mu = \frac{1}{\sqrt{2}}) \\ -1 & (\lambda = -\mu = \frac{-1}{\sqrt{2}}) \end{cases} \quad (6.D.8)$$

It is of notice that, in quantum mechanics, average values imply the mean outcome of a large number of experiments. In this case, of the (simultaneous) measure of the position of the two particles⁵².

Appendix 6.E Correlation length and quantality parameter.

The correlation length can be defined as⁵³

$$\xi = \frac{\hbar v_F}{\pi \Delta} \approx \frac{\hbar^2 k_F}{m \pi \Delta} \quad (6.E.1)$$

where the Fermi momentum in the case of stable nuclei lying along the stability valley is

$$k_F \approx 1.36 \text{ fm}^{-1}. \quad (6.E.2)$$

Thus,

$$\xi = 40 \text{ MeV fm}^2 \times \frac{1.36}{\pi \Delta} \text{ fm}^{-1} \approx \frac{17}{\Delta} \text{ fm}, \quad (6.E.3)$$

and,

$$\xi \approx 14 \text{ fm}, \quad (\Delta \approx 1.2 \text{ MeV}). \quad (6.E.4)$$

Thus, the associated (generalized) quantality parameter is, in the present case:

$$q_\xi = \frac{\hbar^2}{2m\xi^2} \frac{1}{2\Delta} \approx 0.04. \quad (6.E.5)$$

That is, the two partner nucleons are, in the Cooper pair, rigidly correlated with each other.

We now consider $^{11}_3\text{Li}$, and calculate k_F (neutrons) with the help of the Thomas-Fermi model⁵⁴

$$k_F = \left(3\pi^2 \frac{8}{\frac{4\pi}{3}(4.58)^3} \right)^{1/3} \text{ fm}^{-1} \approx \frac{(18\pi)^{1/3}}{4.58} \text{ fm}^{-1} \approx 0.8 \text{ fm}^{-1}. \quad (6.E.6)$$

⁵²Basdevant and Dalibard (2005).

⁵³See e.g. Annert (2013) p. 62.

⁵⁴Quantity which can be related to (v_F/c) according to $v_F/c = \hbar k_F / (mc) = (\hbar c / (mc^2)) k_F \approx 0.2(k_F)$. In the case in which $k_F \approx 0.8 \text{ fm}^{-1}$ (see Eq. (6.E.6)), $v_F/c \approx 0.16$.

fm⁻¹

two

pair removal mode, while those of the vortex exchange pairs of Coopers pairs (monopole pairing vibrations), but also ~~pairs~~ of dipole pairs, as shown in Figs. 6.F.1 and 6.F.2. In other words, by liaising with each other, the two dineutrons contenders at the role of ^{11}Li ground state settle the issue. As a result the Cooper pair becomes weakly bound ($S_{2n} = 380$ keV), the vortex state remaining barely unbound, by about 0.5–1 MeV. There is no physical reason why things could not have gone the other way, at least none that we know. Within this context we refer to ^3He superfluidity, where condensation involve $S = 1$ pairs. It is of notice that we are not considering spin degrees of freedom in the present case, at least not dynamic ones.

For practical purposes, one can describe the 1^- as a two quasiparticle state and calculate it within the framework of QRPA adjusting the strength of the dipole-dipole separable interaction to reproduce the experimental findings (Fig. 3.C.1). In this basis it is referred to as a Pygmy Dipole Resonance (PDR). Exchanged between the two partners of the Cooper pair (Fig. 6.F.1(d)) leads to essentially the right value of dineutron binding to the ^9Li core. Within this context one can view the ^{11}Li neutron halo as a van der Waals Cooper pair (Fig. 6.F.1(e)). The transformation between this picture and that discussed in connection with (a) and (b) as well as with Fig. 6.F.2 can be obtained expressing the PDR-QRPA wavefunction, in terms of particle creation and destruction operators (Bogoliubov-Valatin transformation) as seen from Fig. 6.F.1(a) and (b). A vortex-vortex stabilised Cooper pair emerges.

Which of the two pictures is more adequate to describe the dipole mediated condensation is an open question, as each of them reflects important physical properties which characterise the PDR. In any case, both indicate the symbiotic character of the halo Cooper pair addition mode and of the pygmy resonance built on top of, and almost degenerate with it. Insight into this question can be obtained by shedding light on the question of whether the velocity field of each of the symbiotic states is more similar to that associated with irrotational or vortex-like flow⁶⁴. Two-nucleon transfer reactions, specific probe of (multipole) pairing vibrational modes, contain many of the answers to the above question (Figs. 6.F.3). In fact, ground state correlations will play a very different role in the absolute value of the

⁶⁴See Repko et al. (2013). Within this context, and making use of an analogy, one can mention that a consistent description of the GQR and of the GIQR is obtained assuming that the average eccentricity of neutron orbits is equal to the average eccentricity of the proton orbits (Bès et al. (1975)), the scenario of neutron skin. The isoscalar quadrupole-quadrupole interaction is attractive. Furthermore, the valence orbitals of nuclei have, as a rule and aside from intruder states, homogeneous parity. These facts preclude the GQR to play the role of the GDPR. In fact, there will always be a low-lying quadrupole vibration closely connected with the aligned coupling scheme and thus with nuclear plasticity. Within this context one can nonetheless posit that the GQR, related to neutron skin, is closely associated with the aligned coupling scheme. Making a parallel, one can posit that the GDPR is closely connected with vortical motion. Arguably, support for this picture is provided by the low-lying E1 strength of ^{11}Li . It results from the presence of $s_{1/2}$ and $p_{1/2}$ orbitals almost degenerate and at threshold, leading to a low-lying Cooper pair coupled to angular momentum 1^- . (dipole pair addition mode). The scenario of vortical motion.

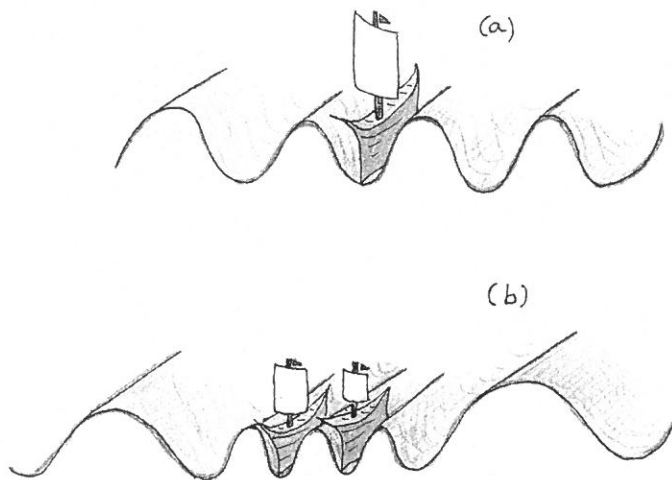


Figure 6.G.2: (Color online) Schematic representation of the behaviour of an isolated ship at sea in a situation of no wind but of strong swell (a), and of two ships close by in similar conditions (b).

circumstances, two vessels at close distance, attracted each other. This in keeping with the fact that the rigs of the rolling ships became often entangled leading to disaster. It was not until quite recently⁶⁷ that a quantitative understanding of the phenomenon (based on knowledge of similar quantal effects) was achieved, providing evidence that the old tale was true. Only waves with wavelength smaller than the separation of the ships can exist between them. In the region of sea extending away from the ships to the horizon, waves of any wavelength can exist (see Fig. 6.G.2(b)). This fact results into an imbalance between the forces exerted by the internal (between ships) waves, in favour of that exerted by the external waves, leading to a net attraction. Quantum mechanical, such an effect is known as the Casimir effect⁶⁸.

Two conducting, neutral plates at very small distances, of the order of the micron ($1\mu = 10^{-6}$ cm), attract each other, due to the imbalance in electromagnetic field pressure exerted by the bombarding of the surface by electrons and positrons, arising from the ZPF of the electromagnetic field⁶⁹ (see Fig. 6.G.3). It is of notice that the Casimir effect, namely the attraction between two metallic, uncharged, plates (which have been drawn in Fig. 6.G.3 as plane surface but which could, in

⁶⁷Boersma (1996).

⁶⁸Casimir (1948).

⁶⁹As stated in the last sentences of the caption to Fig. 6.G.3, long wavelengths play the central role in the Casimir effect. A recurring property of the modes renormalizing the bare interaction or the associated collective variables (elementary modes of excitation) found in condensed matter (phonons of much lower frequency (ω_{lp}) than plasmons (ω_{cp})), nuclei ($\hbar\omega_2$), ($\hbar\omega_{PDE} \ll \hbar\omega_{GR}$) proteins 

(in this connection see Micheletti et al (2001), (2002), (2004), Hamacker (2010) and refs. therein.)

Michelletti, C., Carloni, P. and Mantova, A. (2004) Accurate and efficient description of protein-vibration dynamics and Gaussian model. Protein 55, 385.
 Michelletti, C., Flaminio, F., Cecconi, F., Flaminio, A., Mantova, A. (2002) Conformational states of proteins through folding/unfolding cycles. Proc Natl Acad Sci USA 99, 12788.
 Michelletti, C., Flaminio, F., Cecconi, F., Mantova, A. (2001) Crucial role of protein folding/unfolding cycles in determining target site for HIV-1 protease. J Biophys 79, 1051.
 K. Hamacher, Temperature dependence of fluctuations of proteins

* As stated in the last sentence of the caption to Fig. 6.6.3, long wavelengths play the central role in the Corium effects. A recurrent property found in condensed matter (phonons) of much lower frequency (ω_{ip}) than plasmons (ω_{ep})), nuclei ($\hbar\omega_2$, $\hbar\omega_{\text{DPR}}$ (cf. $\hbar\omega_{\text{GR}}$), prottons (in this connection see Michalek et al (2001), (2002), (2004), Hennacher (2010) and refs. therein)

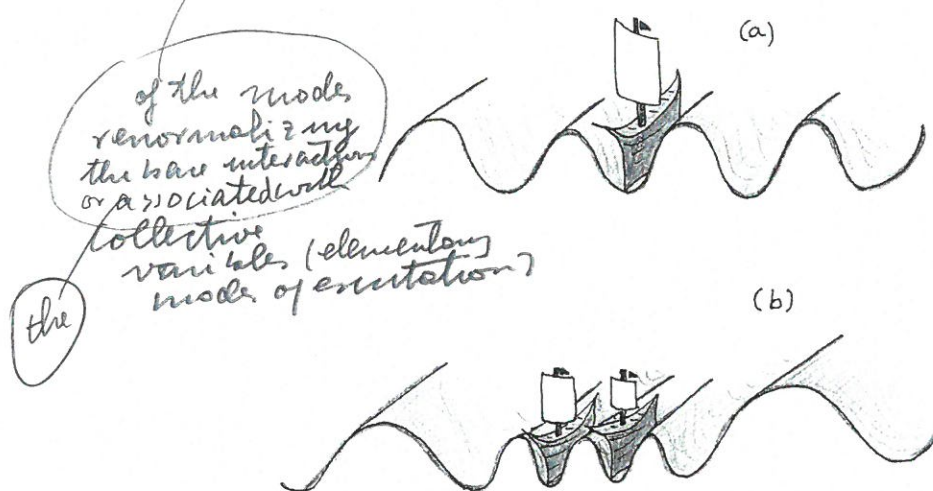


Figure 6.G.2: (Color online) Schematic representation of the behaviour of an isolated ship at sea in a situation of no wind but of strong swell (a), and of two ships close by in similar conditions (b).

circumstances, two vessels at close distance, attracted each other. This in keeping with the fact that the rigs of the rolling ships became often entangled leading to disaster. It was not until quite recently⁶⁸ that a quantitative understanding of the phenomenon (based on knowledge of similar quantal effects) was achieved, providing evidence that the old tale was true. Only waves with wavelength smaller than the separation of the ships can exist between them. In the region of sea extending away from the ships to the horizon, waves of any wavelength can exist (see Fig. 6.G.2(b)). This fact results into an imbalance between the forces exerted by the internal (between ships) waves, in favour of that exerted by the external waves, leading to a net attraction. Quantum mechanical, such an effect is known as the Casimir effect⁶⁹.

Two conducting, neutral plates at very small distances, of the order of the micron ($1\mu = 10^{-6}$ cm), attract each other, due to the imbalance in electromagnetic field pressure exerted by the bombarding of the surface by electrons and positrons, arising from the ZPF of the electromagnetic field (see Fig. 6.G.3). It is of notice that the Casimir effect, namely the attraction between two metallic, uncharged, plates (which have been drawn in Fig. 6.G.3 as plane surface but which could, in principle have any shape) is not so different from that experienced by leptodermic systems, that is, systems which display a surface tension. Setting two of such systems in contact “destroys” part of their surface. But this is tantamount to saying that one has to spend some amount of work to separate the systems from each other,

⁶⁸ Boersma (1996).

⁶⁹Casimir (1948).

*)

Mander Gregory

*) as stated in the last sentence of the caption to Fig. 6.G.3 ,
 long wavelengths play the central role in the Casimir effects. A recurrent property found in condensed matter (phonons) of much lower frequency (wip) than phonons (wep), nuclei (tw_2 , tw_{DR} to tw protein) (in this connection see Micheletti et al (2001), (2002), (2004), Hennacher (2010) and refs.)

490

CHAPTER 6. STRUCTURE WITH TWO NEUTRONS

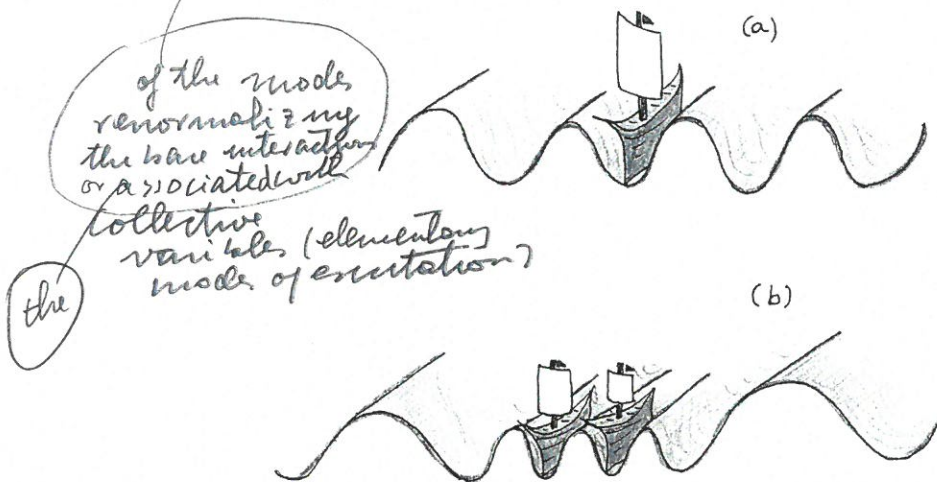


Figure 6.G.2: (Color online) Schematic representation of the behaviour of an isolated ship at sea in a situation of no wind but of strong swell (a), and of two ships close by in similar conditions (b).

circumstances, two vessels at close distance, attracted each other. This in keeping with the fact that the rigs of the rolling ships became often entangled leading to disaster. It was not until quite recently⁶⁸ that a quantitative understanding of the phenomenon (based on knowledge of similar quantal effects) was achieved, providing evidence that the old tale was true. Only waves with wavelength smaller than the separation of the ships can exist between them. In the region of sea extending away from the ships to the horizon, waves of any wavelength can exist (see Fig. 6.G.2(b)). This fact results into an imbalance between the forces exerted by the internal (between ships) waves, in favour of that exerted by the external waves, leading to a net attraction. Quantum mechanical, such an effect is known as the Casimir effect⁶⁹.

Two conducting, neutral plates at very small distances, of the order of the micron ($1\mu = 10^{-6}$ cm), attract each other, due to the imbalance in electromagnetic field pressure exerted by the bombarding of the surface by electrons and positrons, arising from the ZPF of the electromagnetic field (see Fig. 6.G.3). It is of notice that the Casimir effect, namely the attraction between two metallic, uncharged, plates (which have been drawn in Fig. 6.G.3 as plane surface but which could, in principle have any shape) is not so different from that experienced by leptodermic systems, that is, systems which display a surface tension. Setting two of such systems in contact "destroys" part of their surface. But this is tantamount to saying that one has to spend some amount of work to separate the systems from each other,

⁶⁸Boersma (1996).

⁶⁹Casimir (1948).

- Micheletti, C., Carloni, P. and Mantan, A (2004) Accurate and efficient description of systems vibrational dynamics; comparing molecular dynamics and gammon models. *J. Protein* **55**, 365.
 Micheletti, C., Barcaraz, J.B., Mantan, A. (2001) Conformational changes of proteins in equilibrium. *PRB* **87**, 082102-1-7
 Micheletti, C., Flaminini, F., Mantan, A. (2002) Crucial stages of protein folding through inhibiting drug. *Prot. Sci.* **11**, 1878-1895 (2010)
 Micheletti, C., Cecconi, F., Flaminini, F., Mantan, A., Producing target sites for enzyme-mediated binding of HIV 1-protease. *Eur. Biophys. J.* **39**, 1051.

Mandar Gregory

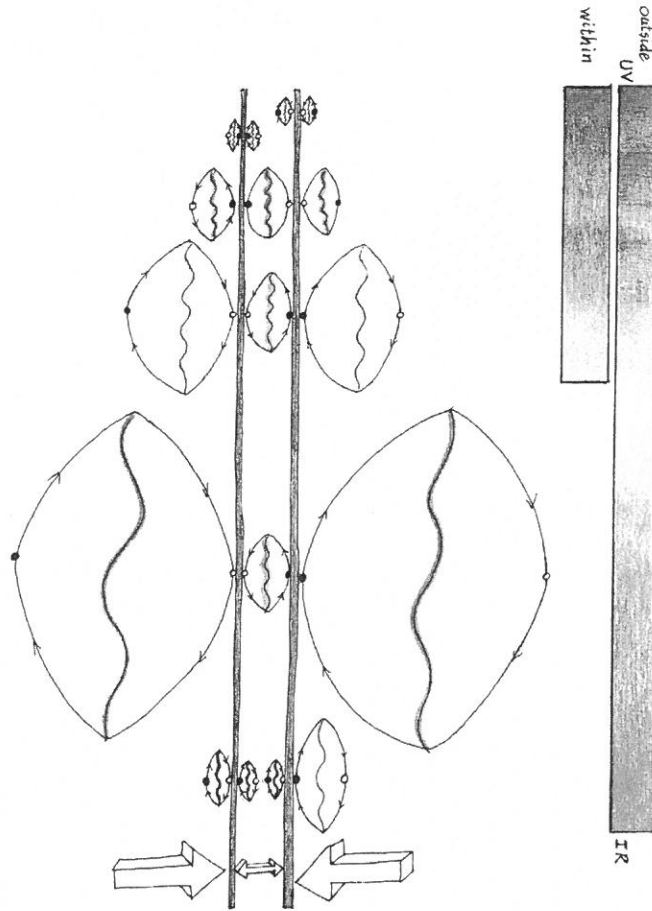


Figure 12.

Figure 6.G.3: (Color online) Casimir effect. Two metallic isolated, conducting plates (grey vertical sections) in vacuum attract each other when they are placed at very small distances (of the order of micron). This is known as the Casimir effect. The origin of such a force are, in this work, traced back to quantal zero point fluctuations (ZPF) of the electromagnetic vacuum. In the figure a cartoon of such processes is given. Virtual electrons (e^- , solid dots) and positrons (e^+ , open dots) pop up of the vacuum together with a photon, travel for short distances on timescales of the order of $\hbar/1\text{MeV} \approx 10^{-23}\text{ s}$ (1 MeV being approximately equal to the summed mass of e^- and e^+). In their way, some of them hit the plates. The different wavelengths of the visible photons (and thus the associate momenta of the fermions), are displayed with the standard color coding of the rainbow. Of course, the spectrum extends beyond such limit (from UV to IR). Because the range of colors (wavelengths) allowed between the plates is smaller than the full spectrum (see colored spectra to the far right of the figure) allowed for the photons associated with the electromagnetic ZPF in the right and left unlimited halves, more fermions or bosons will be knocking the plates from outside than from the in between region, thus leading to an imbalance of the “quantal” pressure and consequently to an effective attractive force. Within this scenario, there are in fact the long wavelengths of the electromagnetic spectrum which are responsible for the attraction between the metallic plates in the Casimir effect. In other words, quantal pressure by infrared.

italics



($|gs\rangle = |1s^2\rangle|2s^2\rangle|2p^4\rangle$). It can thus use at profit the electrons of the two H-atoms to dynamically become a closed shell system (${}^{20}\text{Ne}$ -noble gas-like electronic configuration, Fig. 6.G.5 (c)), a requirement simple to fulfill in the present case. This is in keeping with the fact that the hydrogen atom H is prone to share its electron.

Hybridization between the four orbitals $|2s\rangle$, $|2(p_x)\rangle$, $|2(p_y)\rangle$ and $|2(p_z)\rangle$ leads to a tetrahedral correlation in which the four orbitals $|i\rangle$ point towards the corners of a tetrahedron with the oxygen atom at the center (Fig. 6.G.5 (a), 6.G.6). Because the electronic distribution has its charge center closer to the oxygen atom than to the two protons of the H-atoms, H_2O has a sizable dipole moment⁷² ($\approx 0.68ea_0 \approx 0.6$ D, e being the electron charge, a_0 the Bohr radius and D the Debye unit). Water molecules can form four hydrogen bonds⁷³ (hb), a special bond between molecules which is produced in situations when they share an hydrogen nucleus between them. The molecule's two hydrogen atoms form two bonds with neighboring oxygens, while the molecule's two lone pairs interact with neighboring hydrogens⁷⁴ (Figs. 6.G.5 (b), 6.G.7).

Water and oil do not mix. The term hydrophobic (water-fearing) is commonly used to describe substances that, like oil, do not mix (dissolves) with (in) water. Although it may look as if water repels oil, these two types of molecules actually attract each other, e.g. through the van der Waals interaction, but not nearly as strongly as water attracts itself. Mixing enough oil (hydrophobic, non polar (NP) molecules) with water leads to a reduction in favorable bonding. Strong mutual attraction between water molecules induce segregation of NP molecules from water and results in an effective NP-NP (hydrophobic) attraction, as observed e.g. in surface force measurements⁷⁵. For example, the loss of hydrogen bonds near the two extended hydrophobic surfaces depicted in Fig. 6.G.8 causes water to move

⁷²The dipole moment of a polar molecule is defined as $\mu = ql$, where l is the distance between the two charges $+q$ and $-q$. Thus, for two electronic charges $q = \pm e$ separated by $l = 0.1$ nm, the dipole moment is $\mu = 1.602 \times 10^{-19} \text{ C} \times 10^{-10} \text{ m} = 4.8 \text{ D}$, where the Debye=1D=3.336×10⁻³⁰ Cm is the unit of dipole moment. Small polar molecules have moments of the order of 1D (see e.g. Israelachvili (1985)).

⁷³Let us consider an H atom in a covalent bond with oxygen. When a second oxygen atom approaches the H atom, its nucleus, the proton, sees a potential with two minima, and tunnels through the corresponding barrier from one minimum to the other. In other words, the effective potential in which the proton moves becomes broader as compared to the single oxygen potential. Thus, the quantum mechanical confinement kinetic energy decreases by roughly a factor of two. This implies that the order of magnitude energy of an hydrogen bond between two oxygen atoms corresponds to the difference in the corresponding ZPF energies, i.e. ≈ 200 meV ($\approx 0.38 \text{ eV} - 0.19 \text{ eV} \approx 0.2 \text{ eV} \approx 4.6 \text{ kcal/mol} \approx 8 \text{ kT}$), where kT ($\approx 0.6 \text{ kcal/mol} \approx 27 \text{ meV}$) is the thermal energy at room temperature ($\approx 310 \text{ K}$). For comparison a covalent bond corresponds to $\approx 96 \text{ kcal/mol} \approx 4 \text{ eV}$, while the van der Waals interaction energy between two H at a distance of 2.4 Å, that is of the order of the hydrogen bond length of 1.83 Å, is ≈ 20 meV (see Povh and Rosina (2002)).

⁷⁴A possible pedestrian explanation of this is to impersonate a water molecule. Quoting from Ball (2003): "Your hands are hydrogen atoms, your ankles are the lone pairs of electrons of oxygen. Stand legs apart... Twist 90° at the waist, stretch your arms and you're H_2O . The way that water molecules join up has just one rule: hands can grab ankles, but nothing else. That grasp is an hydrogen bond".

⁷⁵See e.g. Chandler (2002, 2005) and Lum et al. (1999) and references therein.

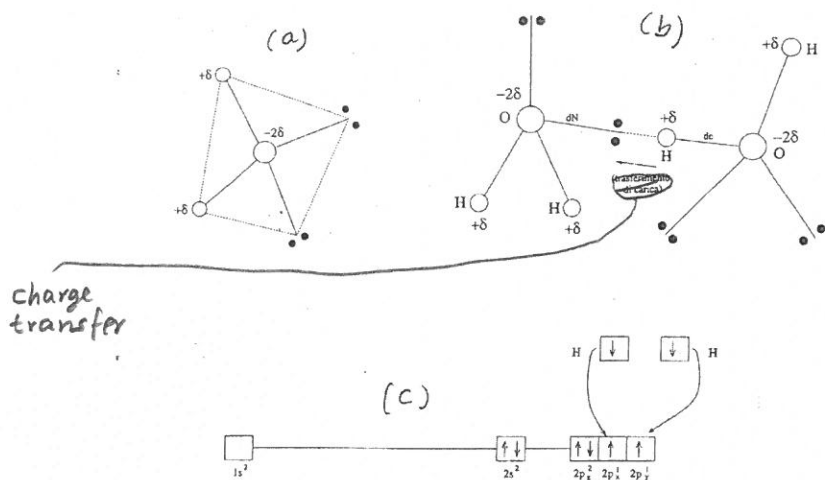


Figure 6.G.5: (a) To understand the behavior of water molecules one has to realize that in the covalent bonds, where the oxygen and the hydrogen atoms share a couple of electrons, the corresponding electronic cloud is somewhat more concentrated on the oxygen than on the hydrogen. The oxygen acquires a partial charge $-2δ$ while each hydrogen gets a positive one $+δ$. (b) Such charges give rise to an attractive electric force between close lying molecules, in which the hydrogen atoms of a molecule points to the oxygen atom of the other molecule. One can view this attractive force as a type of chemical bond. It is known as hydrogen bond. It is of notice that also in this type of bond there is a component which implies the sharing of electrons. Furthermore, the hydrogen atom in an hydrogen bond does not just stick indiscriminantly to the the oxygen of another molecule. Being positively charged it goes where the electrons are. So the hydrogen bond is a bond between a hydrogen atom and a lone pair (two bold face dots). This means that a water molecule can form four hydrogen bonds: the molecule's two hydrogens form two bonds with neighboring oxygens, while the molecule's two lone pairs interact with neighboring hydrogens. (c) Schematic electronic structure of H_2O .